metals

MDPI

Article

Effect of Annealing Temperature on the Corrosion Protection of Hot Swaged Ti-54M Alloy in 2 M HCl Pickling Solutions

El-Sayed M. Sherif [1,2,*], Ehab A. El Danaf [3], Hany S. Abdo [1,4], Sherif Zein El Abedin [2] and Hasan Al-Khazraji [5]

1 Deanship of Scientific Research, Advanced Manufacturing Institute (AMI), King Saud University, P.O. Box 800, Al-Riyadh 11421, Saudi Arabia; habdo@ksu.edu.sa
2 Electrochemistry and Corrosion Laboratory, Department of Physical Chemistry, National Research Centre, El-Behoth St. 33, Dokki, 12622 Cairo, Egypt; sherifzein888@yahoo.com
3 Mechanical Engineering Department, College of Engineering, King Saud University, P.O. Box 800, Al-Riyadh 11421, Saudi Arabia; edanaf@ksu.edu.sa
4 Mechanical Design and Materials Department, Faculty of Energy Engineering, Aswan University, Aswan 81521, Egypt
5 Former Ph.D. Student at Institute of Materials Science and Engineering, Clausthal University of Technology, Clausthal-Zellerfeld 38678, Germany; hamedhasan10@gmail.com
* Correspondence: esherif@ksu.edu.sa; Tel.: +966-114699668

Academic Editor: Hugo F. Lopez
Received: 13 November 2016; Accepted: 11 January 2017; Published: 20 January 2017

Abstract: The corrosion of Ti-54M titanium alloy processed by hot rotary swaging and post-annealed to yield different grain sizes, in 2 M HCl solutions is reported. Two annealing temperatures of 800 °C and 940 °C, followed by air cooling and furnace cooling were used to give homogeneous grain structures of 1.5 and 5 μm, respectively. It has been found that annealing the alloy at 800 °C decreased the corrosion of the alloy, with respect to the hot swaged condition, through increasing its corrosion resistance and decreasing the corrosion current and corrosion rate. Increasing the annealing temperature to 940 °C further decreased the corrosion of the alloy.

Keywords: titanium alloys; annealing; corrosion; pickling solutions; EIS; polarization

1. Introduction

Titanium and its alloys have many applications in industry for their good properties. These materials have excellent ballistic, fatigue, and corrosion resistances, low Young's modulus, high yield strength, ultimate tensile strength, and sufficient ductility [1]. These alloys have been used in automobiles, aircrafts, armors, different implant systems, in motorcycles with higher power engines, etc. [2–6]. It has been reported [7] that titanium armor provides a 15%–35% weight savings when compared to steel or aluminum armor for the same ballistic protection at areal densities of interest, which has resulted in substantial weight savings on military ground combat vehicles. Titanium has a very tenacious nascent oxide that is formed instantly on its surface upon exposure to air. The excellent corrosion resistance, low ferromagnetism, and compatibility with composites also provide significant benefits.

Titanium alloys are known to be one of the most difficult materials to machine [1]. This is due to their low thermal conductivity, which causes high cutting temperatures. Moreover, the low elastic modulus of titanium alloys leads to tool vibrations during chip formation. Several researchers have reported that the machining of titanium alloys is one of the principal challenges for their application [8–12]. Developing new kinds of titanium alloys with increased machinability has been

reported [13,14]. TIMET developed a new alloy named TIMETAL54M (Ti-54M), which is an α-β alloy. Ti-54M alloy has been developed with superior machinability and strength to replace the widely-used Ti-6Al-4V alloy [10,15,16].

The corrosion of Ti-54M alloy in most known corrosive media is not available. Divi and Gruman [16] have reported the electrochemical corrosion behavior of Ti-54M in some corrosive media, including reducing, oxidizing, and chloride ones, using linear polarization resistance and potentiodynamic polarization techniques. It was claimed that the general corrosion behavior of Ti-54M and Ti-6Al-4V alloys are mostly likely similar. The authors [16] also used hydrogen uptake efficiency (HUE) technique in acidic chloride containing solutions and found that Ti-54M alloy has much lower HUE than Ti-6Al-4V. Moreover, the repassivation potential for the Ti-54M alloy was much better than Ti-6Al-4V alloy under chloride and reducing environments.

In the present study, the corrosion behavior of hot swaged Ti-54M alloy after 1.0 h and 24.0 h immersion in 2 M HCl solutions has been investigated. The effect of post swaging annealing temperatures of 800 °C and 940 °C on the protection of Ti-54M alloy against corrosion at the same conditions was also reported. Electrochemical impedance spectroscopy, cyclic potentiodynamic polarization, and chronoamperometric current-time were the corrosion test methods in this study. The work was complemented using scanning electron microscope images and energy-dispersive X-ray analysis. It is expected that the annealing of this alloy at the different temperatures, 800 °C and 940 °C, would increase its corrosion resistance in the acidic test solutions.

2. Materials and Methods

Ti-54M alloy, having (α + β) phase, was investigated in this study. This alloy was received as hot extruded bar, having a duplex microstructure and chemical composition (wt %) of 5.03% Al, 3.95% V, 0.57% Mo, 0.51% Fe, 0.11% Si, 0.10% C, 0.06% O, 0.05% N, 0.005% Zr, and the rest was Ti. A rotary swaging (RS) technique at 850 °C and a deformation degree of 3.0 was used to process this alloy. The cross-sectional area reduction, $\varepsilon_t = \ln \frac{A_0}{A}$, where A_0 is the initial cross-section and A is the final cross-section area, was used to calculate the true strain. Details of this processing technique are illustrated elsewhere [17]. Specimens, from the swaged bar were taken in the transverse direction and subjected to two heat treatment conditions. This was to obtain two differently-sized equiaxed microstructures by annealing at 800 and 940 °C for 1.0 h. The annealed samples were subjected to air cooling and furnace cooling, respectively, to yield an average grain size of 1.5 and 5 μm, respectively. The hot swaged condition exhibited an average grain size of 1.6 μm. All materials were given a final heat treatment at 500 °C for 24 h to age-harden the α phase by Ti3Al precipitates and the β phase by fine secondary α precipitates.

Hydrochloric acid (HCl, 32%) was purchased from Glassworld (Johannesburg, South Africa) and used as received. The test solution, 2 M HCl, was prepared from the stock HCl solution by dilution. All corrosion tests were carried out in a conventional three-electrode electrochemical cell accommodating for 350 mL of the test solution. An Ag/AgCl, a platinum foil, and the Ti-54M alloys were employed as the reference, counter, and working electrodes, respectively. The working electrode was prepared by welding a copper wire to one surface of the Ti-54M alloy. The sample was then mounted in an epoxy resin and one only surface was ground and exposed to the chloride acid test solution. The surface to be exposed to the solution was ground successively with metallographic emery paper of increasing fineness of up to 1000 grit.

An Autolab potentiostat-galvanostat operated by the general purpose electrochemical software (GPES, version 4.9, Amsterdam, The Netherlands) was used to perform the electrochemical measurements. The electrochemical impedance spectroscopy (EIS) measurements were performed at corrosion potentials over a change of frequency from 100 kHz to 100 mHz, with an AC wave of ±5 mV peak-to-peak overlaid on a DC bias potential, and the impedance data were collected using Powersine software at a rate of 10 points per decade change in frequency. The cyclic potentiodynamic polarization (CPP) measurements were carried out by scanning the potential from −1000 mV in the

positive direction to 1800 mV at a scan rate of 3 mV/s. The potential was scanned in the backward direction at the same scan rate just after the forward scan. The change of current versus time at constant positive potential experiments were carried out by stabilizing the potential of the working electrodes at 1400 mV. All measurements were conducted after immersing our working electrodes in the hydrochloric acid solutions for 1.0 h and 24 h at room temperature. A new portion of the acid solution and a fresh surface of the alloys were employed in each experiment. SEM micrographs were obtained using a field emission scanning electron microscope (FE-SEM) Model JSM-7600F supplied by JEOL (Tokyo, Japan) after performing chronoamperometric current time experiments after 24 h immersion in 2 M HCl solutions. The applied voltage during SEM imaging was 15 kV.

3. Results and Discussion

3.1. Electrochemical Impedance Spectroscopy (EIS) Measurements

EIS method has been successfully employed to report the kinetic parameters for metals and alloys exposed to harsh environments [18–21]. The Nyquist plots obtained for (1) hot swaged; (2) annealed at 800 °C; and (3) annealed at 940 °C Ti-45M electrodes after their immersion for 1.0 h in 2 M HCl solutions are shown in Figure 1. Similar plots were also obtained for the same materials after 24 h immersion in the acid solution and depicted in Figure 2. The EIS data shown in Figures 1 and 2 were fitted to the best equivalent circuit that is shown in Figure 3. The values of the elements of the equivalent circuit (Figure 3) were obtained and listed in Table 1. The elements of this circuit can be defined as follows; R_S is the solution resistance, Q (CPEs) is the constant phase elements, R_{P1} is the polarization resistance between the surface of the alloy and a layer that may form on its surface, and R_{P2} is the polarization resistance of the interface between the surface formed layer and the hydrochloride acid solution.

It is clearly seen from Figures 1 and 2, whether after 1.0 h or 24 h immersion in the acid solution, that there is only one distorted semicircle. The diameter of the semicircle was noticed to increase with heat treating the sample at 800 °C, and further to 940 °C. It is generally agreed that the wider the diameter of the semicircle, the higher the corrosion resistance of the alloy. From this point of view, the resistance of Ti-54M increases with the increase of the annealing temperature. Prolonging the immersion time to 24 h (Figure 2) is noticed to decrease the diameter of the semicircle, which increases with the increase of annealing temperature to 800 °C, and further to 940 °C. This was further confirmed by the data listed in Table 1, where the lowest values of R_S, R_{P1}, and R_{P2} were recorded for the hot swaged alloy and increased with increasing the annealing temperature. The CPEs exponent n values vary from 0.69 to 0.77 revealing that CPEs represent a near capacitance. This is because the values of n values are known to be between 0 and 1; i.e., $0 \leq n \leq 1$, where $n = 1$ is a pure capacitance, $n = 0$ is a pure resistance and $n = 0.5$ is a Warburg element. The values of n in our study, thus, indicate that the surface of the alloys have some pores from which some dissolution occurs under the aggressiveness action of the acid solution. Moreover, the values of the CPEs decreased with the increase of annealing temperature due to the covering of the charged surfaces in order to reduce the capacitive loops. This was also confirmed by the presence of C_{dl}; the value of the C_{dl} also decreased with the annealing temperature. Increasing the exposure period of time to 24 h decreased the values of all resistances (R_S, R_{P1}, and R_{P2}) and slightly increased the values of CPEs and C_{dl} for the three alloys. This indicates that the increase of the exposure period to 24 h before measurements increases the corrosion of the alloys under investigation. However, the resistance against corrosion for these alloys whether it was immersed for 1.0 h or 24 h in the HCl solutions was found to increase according to the annealing temperature in the following order; Ti-45M annealed at 940 °C > Ti-45M annealed at 800 °C > hot swaged Ti-45M alloy.

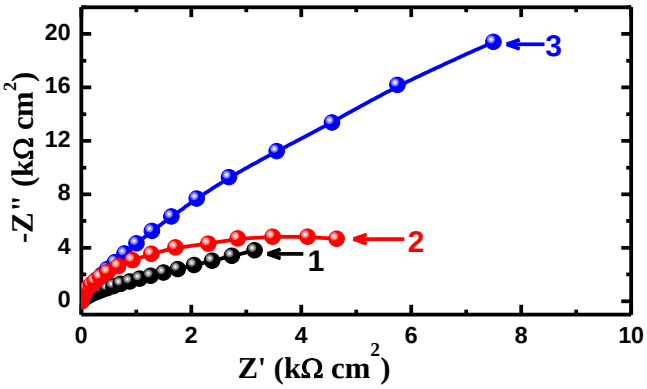

Figure 1. Nyquist plots obtained for (1) hot swaged; (2) annealed at 800 °C; and (3) annealed at 940 °C Ti-45M electrodes after their immersion for 1.0 h in 2 M HCl solutions.

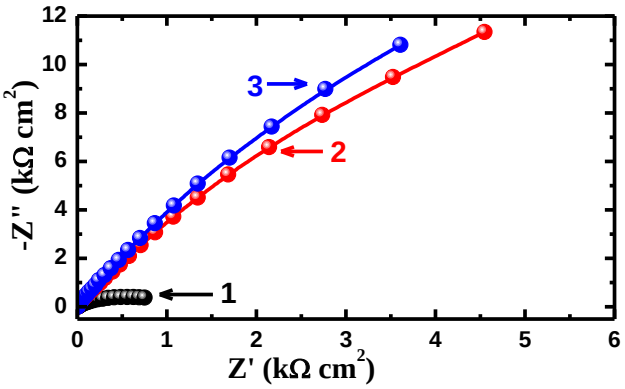

Figure 2. Nyquist plots obtained for (1) hot swaged; (2) annealed at 800 °C and (3) annealed at 940 °C Ti-45M electrodes after their immersion for 24 h in 2 M HCl solutions.

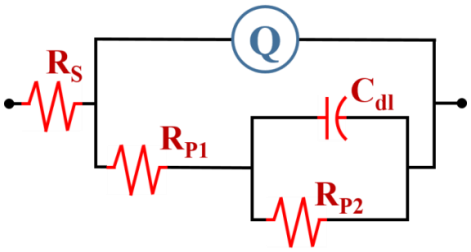

Figure 3. The equivalent circuit model used to fit EIS data shown in Figures 1 and 2.

Table 1. Electrochemical impedance spectroscopy parameters obtained for the different Ti-54M alloys in 2M HCl solutions.

Sample	EIS Parameter					
	R_S (Ω)	Q		R_{P1} (Ω)	C_{dl} (F)	R_{P2} (Ω)
		Y_{Q1} (F·cm^2)	n			
Ti-54M-HS (1 h)	1.038	0.0001378	0.73	2738	0.004712	1755
Ti-54M-800 °C (1 h)	1.739	0.0001305	0.75	3669	0.003907	4322
Ti-54M-940 °C (1 h)	1.999	0.0000385	0.77	4046	0.003146	5618
Ti-54M-HS (24 h)	1.012	0.0007654	0.70	1079	0.005547	1330
Ti-54M-800 °C (24 h)	1.357	0.0000882	0.69	2866	0.004748	3276
Ti-54M-940 °C (24 h)	1.550	0.0000791	0.72	3932	0.004316	4927

Typical Bode (a) impedance of the interface, |Z|, and (b) phase angle plots obtained for Ti-45M electrodes, (1) hot swaged; (2) annealed at 800 °C; and (3) annealed at 940 °C, after their immersion for 1.0 h in 2 M HCl solutions are shown in Figure 4. Similar Bode plots were obtained after 24 h immersion in the acid solutions and depicted in Figure 5. It is clearly seen from Figure 4 that the highest impedance value and the maximum degree of phase angle were recorded for the Ti-54M alloy that was annealed at 940 °C, followed by the alloy that was annealed at 800 °C, and the lowest was for the hot swaged alloy. Increasing the immersion time to 24 h shows almost the same behavior, but with slightly lower values for all treated alloys. This confirms that the corrosion decreases with the increase of the annealing temperature, and also that the increase of the immersion time increases the corrosion of Ti-54M alloys, whether it was hot swaged or annealed.

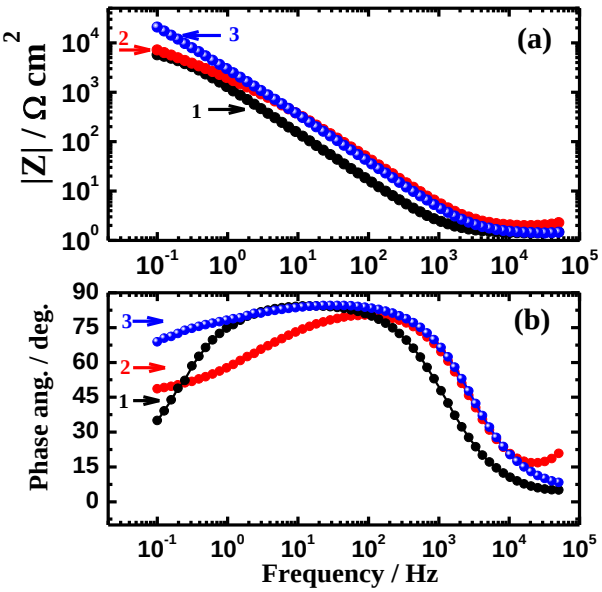

Figure 4. Typical Bode (**a**) impedance of the interface, |Z|; and (**b**) phase angle plots obtained for (1) hot swaged; (2) annealed at 800 °C; and (3) annealed at 940 °C Ti-45M electrodes after their immersion for 1.0 h in 2 M HCl solutions.

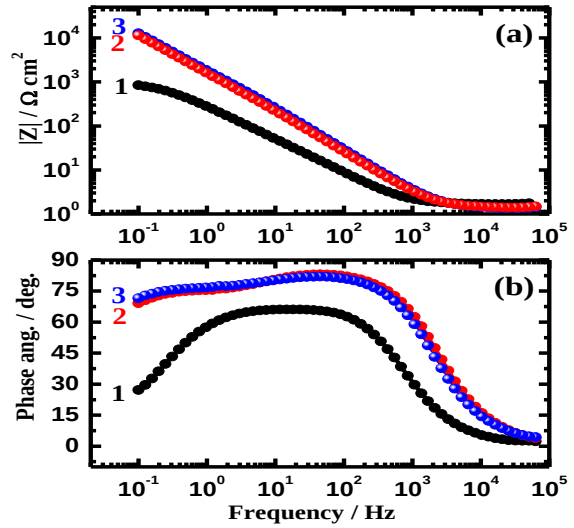

Figure 5. Typical Bode (**a**) impedance of the interface, |Z|; and (**b**) phase angle plots obtained for (1) hot swaged; (2) annealed at 800 °C; and (3) annealed at 940 °C Ti-45M electrodes after their immersion for 24 h in 2 M HCl solutions.

The increase of the corrosion resistance with the increase of the annealing temperature and its relation to the change of the grain size of the alloy can be explained here. The grain size exhibited by the sample that was hot swaged was about 1.6 μm with a high percentage of low-angle grain boundaries of 70%. This indicates the existence of high dislocation density positioned at cell boundaries or, in other words, the microstructure is characterized by a cell structure with low-angle grain boundaries. Annealing the hot swaged alloy for 800 °C, followed by air cooling, resulted in almost similar grain size with a much lower percentage of low-angle grain boundaries of 26%. This point towards reallocation of dislocations by means of the cell boundaries evolved into high-angle grain boundaries, which consumes the high dislocation density. Annealing the hot swaged alloy for 900 °C, followed by furnace cooling, resulted in a relatively higher grain size of 5 μm and an even lower percentage of low-angle grain boundaries of 18%, which points towards further reduction of dislocation density. Therefore, the increase of corrosion resistance of the hot swaged alloy after its annealing at 800 °C and the further increases at 900 °C could be due to the homogeneous distribution of dislocations at grain boundaries, which eliminates, to a great extent, the possibility of creating galvanic cells.

3.2. Cyclic Potentiodynamic Polarization

Cyclic potentiodynamic polarization (CPP) measurements have been widely used to explain the mechanism of corrosion and corrosion protection for metals and alloys in corrosive environments [18–21]. Figure 6 shows the CPP curves obtained for (a) hot swaged, (b) annealed at 800 °C, and (c) annealed at 940 °C Ti-45M electrodes after their immersion for 1.0 h in 2 M HCl solutions. It is seen from Figure 6 that the cathodic currents decreased towards the corrosion current density (j_{Corr}) with increasing the applied potential towards the less negative values. The cathodic reaction at this condition has been reported to the evolution of hydrogen as per the following equation [18,19,22],

$$2H^+ + 2e^- = H_2 \quad (1)$$

The hydrogen gas produced here evolves leaving the acid solution, which, in turn, consumes more electrons and accelerates the dissolution reactions. The current rapidly increased in the anodic branch with little increase in the applied potential due to the occurrence of the anodic reaction, which, in most cases, is the dissolution of the surface and the release of electrons. The recorded current for all treated Ti-54M samples stays almost unchanged with the increase of the applied potential from −0.4 V and up to 1.8 V (Ag/AgCl). This is most probably due to the high corrosion resistance of the alloy, which allows the surface to resist the corrosive action of the concentrated 2 M HCl solution. Back scanning the applied potential produces less currents compared to the obtained currents in the forward direction, which confirms that the pitting corrosion does not occur at this condition.

In order to report the effect of prolonging the immersion time on the corrosion of the different Ti-54M electrodes in 2 M HCl solutions, CPP measurements were also performed after 24 h immersion in 2 M HCl solution and the curves are shown in Figure 7. Although prolonging the immersion time to 24 h does not change the polarization behavior of the Ti-54M in HCl solutions, it increases the corrosion of the tested alloys. The effect of 2 M HCl solutions on the corrosion of hot swaged, annealed at 800 °C, and annealed at 940 °C Ti-54M was quantified via calculating the corrosion parameters obtained from the polarization curves shown in Figures 6 and 7 as listed in Table 2. These parameters are the cathodic Tafel (β_c) slope, anodic Tafel (β_a) slope, corrosion potential (E_{Corr}), corrosion current density (j_{Corr}), polarization resistance (R_P), and corrosion rate (R_{Corr}). The values of E_{Corr} and j_{Corr} were obtained from the extrapolation of anodic and cathodic Tafel lines located next to the linearized current regions. Additionally, the values of R_P were calculated using the Stern-Geary equation as following [23,24]:

$$R_P = \frac{1}{j_{Corr}} \left(\frac{\beta_c \, \beta_a}{2.3 \, (\beta_c \, \beta_a)} \right) \quad (2)$$

Moreover, the values of R_{Corr} (milli-inches per year, mpy) were obtained using the following equation [25]:

$$R_{Corr} = j_{Corr}\left(\frac{k\,E_W}{d\,A}\right) \quad (3)$$

where k is a constant that defines the units for the corrosion rate (k = 3272), E_W is the equivalent weight in grams/equivalent of the alloy (E_W = 11.46 calculated), d is the density in gcm^{-3} (d = 4.43), and A is the area of electrode in cm^2 (A = 1).

It is seen from Table 2 that the value of j_{Corr} and consequently the value of R_{Corr} was the highest for the hot swaged sample and then decreased with an increase in the annealing temperature, while the values of R_P were oppositely increasing. Additionally, the increase of immersion time to 24 h led to significantly increasing the values of j_{Corr} and R_{Corr} for all tested Ti-54M electrodes, and these values decrease with the increase in the annealing temperature. This indicates that increasing the annealing temperature decreases the corrosion of Ti-54M alloy, while the increase of the time of the immersion periods increases its corrosion in 2 M HCl solutions, and that is in good agreement with the data obtained by EIS experiments.

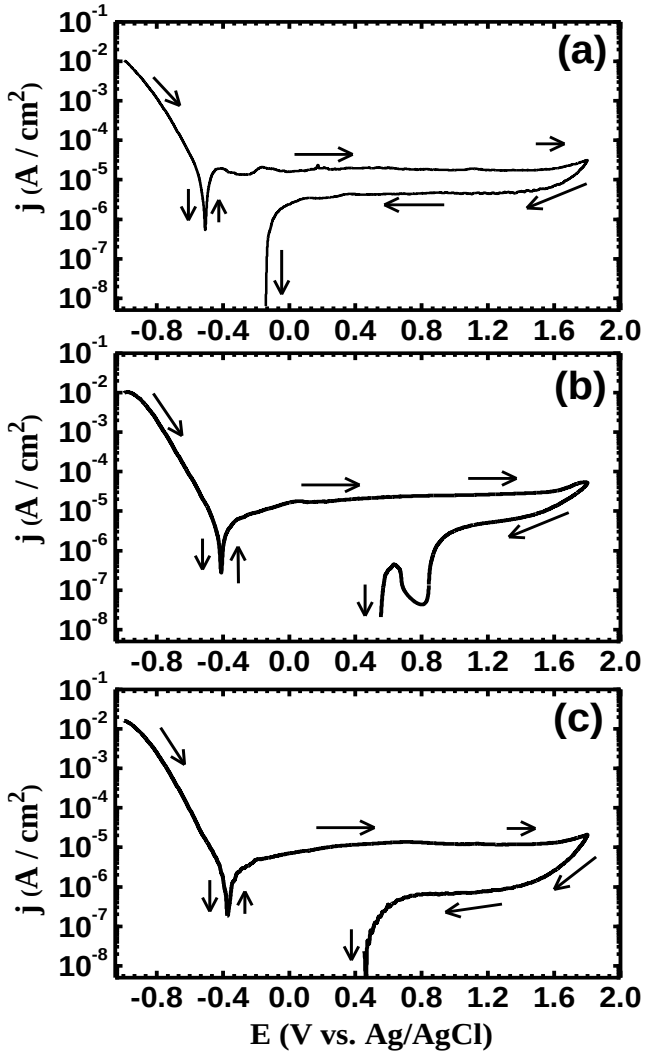

Figure 6. Cyclic potentiodynamic polarization curves obtained for (**a**) hot swaged; (**b**) annealed at 800 °C; and (**c**) annealed at 940 °C Ti-45M electrodes after their immersion for 1.0 h in 2 M HCl solutions.

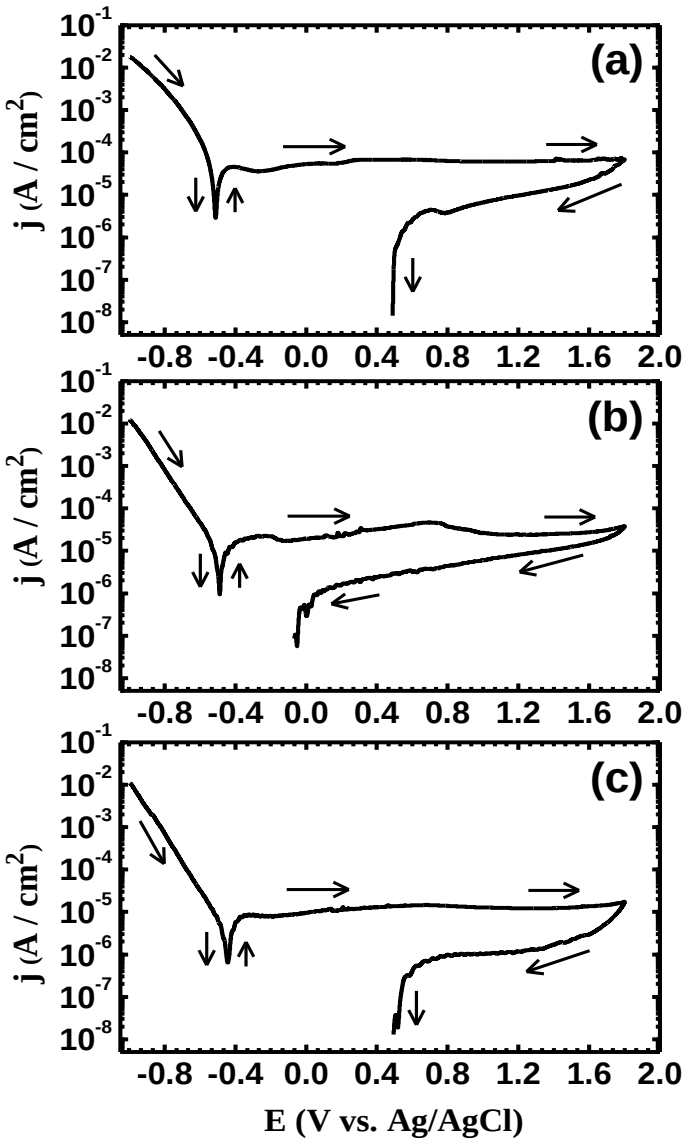

Figure 7. Cyclic potentiodynamic polarization curves obtained for (**a**) hot swaged; (**b**) annealed at 800 °C; and (**c**) annealed at 940 °C Ti-45M electrodes after their immersion for 24 h in 2 M HCl solutions.

Table 2. Parameters obtained from the polarization curves for the different Ti-54M alloys in 2 M HCl solutions.

Sample	Corrosion Parameter					
	β_c (V/dec^{-1})	E_{Corr} (V)	β_a (V/dec^{-1})	j_{Corr} (μA·cm^{-2})	R_p (Ω)	R_{Corr} (mpy)
Ti-54M-HS (1 h)	0.150	–0.515	0.400	12.0	3953	0.1016
Ti-54M-800 °C (1 h)	0.145	–0.390	0.400	4.6	10,059	0.0389
Ti-54M-940 °C (1 h)	0.135	–0.367	0.395	2.2	19,884	0.0186
Ti-54M-HS (24 h)	0.145	–0.472	0.295	38.0	1112	0.3216
Ti-54M-800 °C (24 h)	0.155	–0.470	0.320	9.0	5044	0.0762
Ti-54M-940 °C (24 h)	0.155	–0.460	0.325	4.5	10,140	0.0381

3.3. Chronoamperometric Current-Time Measurements

We have been using chronoamperometric current-time at constant anodic potential experiments to shed more light into whether pitting corrosion occurs for metals and alloys in aggressive media [18–22]. The applied potential value is usually chosen from the anodic polarization branch. Figure 8 shows the

chronoamperometric curves obtained for Ti-45M electrodes, (1) hot swaged; (2) annealed at 800 °C; and (3) annealed at 940 °C, after their immersions in 2 M HCl for 1 h, respectively, followed by stepping the potential to +1.4 V vs. Ag/AgCl for 1.0 h. The same measurements were carried out for the Ti-54M alloys after 24 h immersion in the acid solutions as shown in Figure 9. This current-time technique was employed to confirm whether pitting corrosion takes place for the tested alloy in the acid solutions and also to report the effect of increasing immersion time before measurements on the intensity of both uniform and pitting corrosion. It is seen from Figure 8 that the current increased for Ti-54M hot swaged alloy after its immersion for 1.0 h (curve 1), then the current rapidly decreased, as it did for all heat-treated alloys, from the first moment of applying potential until the end of the run. It is also seen that the increase of the annealing temperature led to a decrease in the absolute values of current with time, where the lowest current values were obtained for the Ti-54M alloy that was annealed at 940 °C (curve 3).

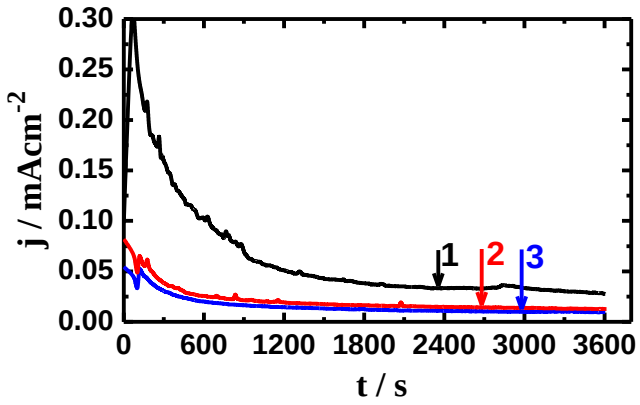

Figure 8. Chronoamperometric curves obtained for (1) hot swaged; (2) annealed at 800 °C; and (3) annealed at 940 °C Ti-45M electrodes after their immersions in 2 M HCl for 1 h, respectively, followed by stepping the potential to +1.4 V vs. Ag/AgCl for 1.0 h.

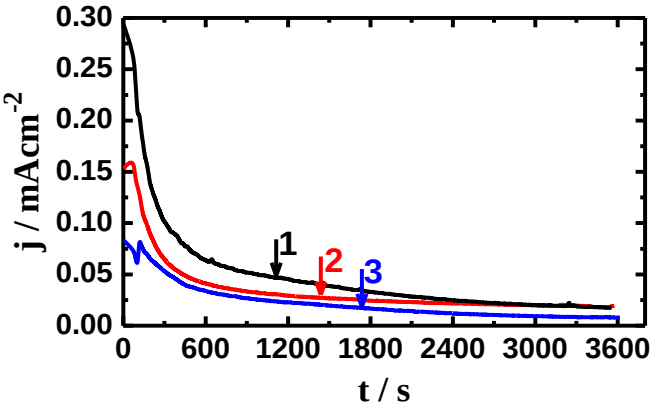

Figure 9. Chronoamperometric curves obtained for (1) hot swaged; (2) annealed at 800 °C; and (3) annealed at 940 °C Ti-45M electrodes after their immersions in 2 M HCl for 24 h, respectively, followed by stepping the potential to +1.4 V vs. Ag/AgCl for 1.0 h.

Prolonging the immersion time to 24 h showed almost the same current-time behavior with higher absolute current values for all investigated alloys. This indicates that increasing the immersion time from 1.0 h to 24 h increases the severity of the uniform corrosion via increasing the absolute current values. Moreover, and although the applied potential was very high value (+1.4 V), this current-time behavior does not give any indications on the occurrence of pitting corrosion of any of the heat-treated

Ti-54M alloys. Where the current values did not increase with time, there are no fluctuations that appear on the values of currents. The chronoamperometric current-time measurements, thus, are in good agreement with the cyclic potentiodynamic polarization data for all Ti-54M alloys at the same conditions.

3.4. Scanning Electron Microscope (SEM) and X-ray Energy Dispersive Spectroscopy (EDX)

In order to report the effect of 2 M HCl solutions on the morphology of the Ti-54M alloys, SEM micrographs and EDX spectra were carried out after immersing Ti-54M alloy in the three conditions mentioned earlier for five days in the acid solutions. Figure 10a,b shows SEM micrographs at different magnifications for the surface of the hot swaged Ti-54M alloy, Figure 10c shows the EDX spectra for the dark areas depicted on the SEM image shown in Figure 10b, and Figure 10d shows the EDX spectra for the white areas of SEM image shown in Figure 10b. Figures 11 and 12 show the SEM images and EDX spectra obtained for Ti-54M alloys annealed at 800 °C and 940 °C, respectively. It is seen from the image shown in Figure 10a that the morphology of the hot swaged alloy is smooth and homogeneous, while the image in Figure 10b declares that the surface developed layers of corrosion products (white areas). The weight percentage of the elements obtained from the EDX spectra for the dark areas (Figure 10c) recorded 93.12% Ti, 4.37% Al, and 2.52% V. On the other hand, the elements obtained for the white areas (Figure 10d) were 78.44% Ti, 2.70% Al, 11.98% V, 3.88% Mo, 2.31% Fe, 0.29% Cl, 0.23% Ca, and 0.18% Pt. The obtained weight percentages thus indicate that the surface of the dark areas contains the main elements of the alloy. At the same time, the low percentages of Ti and Al and the high percent of V, in addition to the presence of Cl recorded for the white areas, indicate that these areas represent thin films of corrosion products and confirm also that the hot swaged alloy does not suffer severe corrosion in the high concentration of the 2M HCl solution.

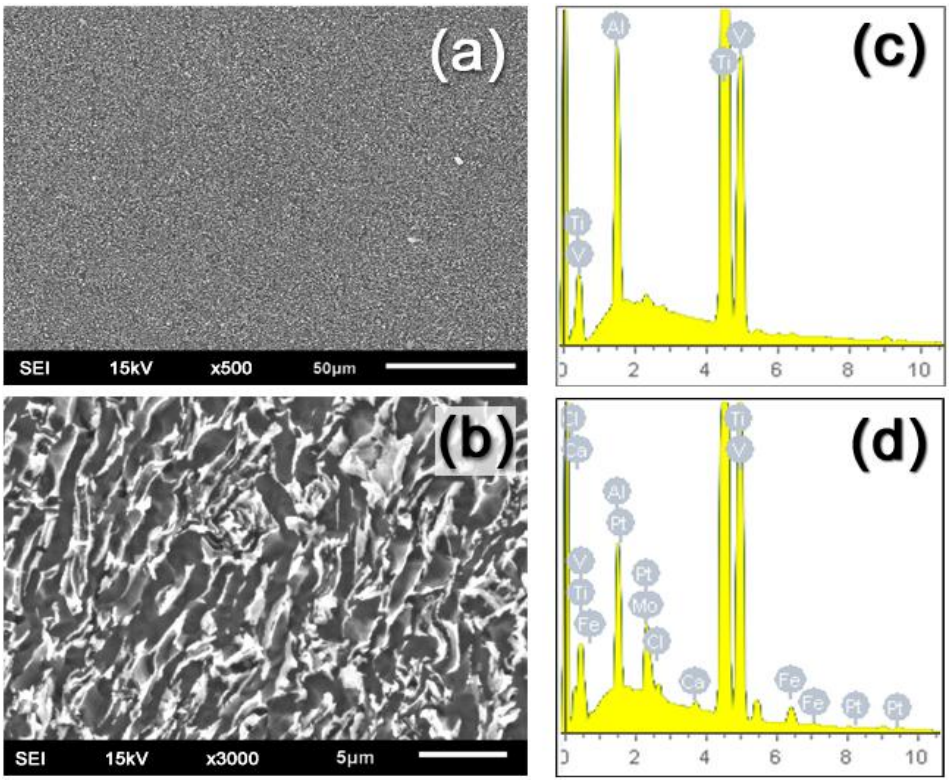

Figure 10. SEM/EDX for the as hot swaged Ti-54M sample after five days of immersion in 2 M HCl solutions, (**a**,**b**) are the SEM images; (**c**,**d**) are the EDX profiles for the area shown in (**a**,**b**), respectively.

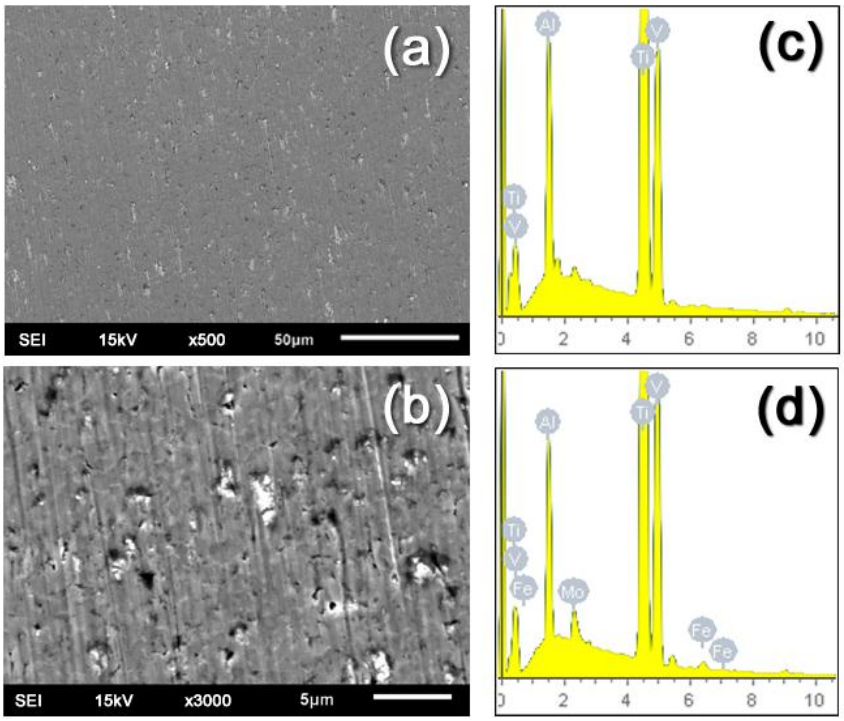

Figure 11. SEM/EDX for the as-annealed Ti-54M sample at 800 °C and after five days of immersion in 2 M HCl solutions, (**a**,**b**) are the SEM images; (**c**,**d**) are the EDX profiles for the area shown in (**a**,**b**), respectively.

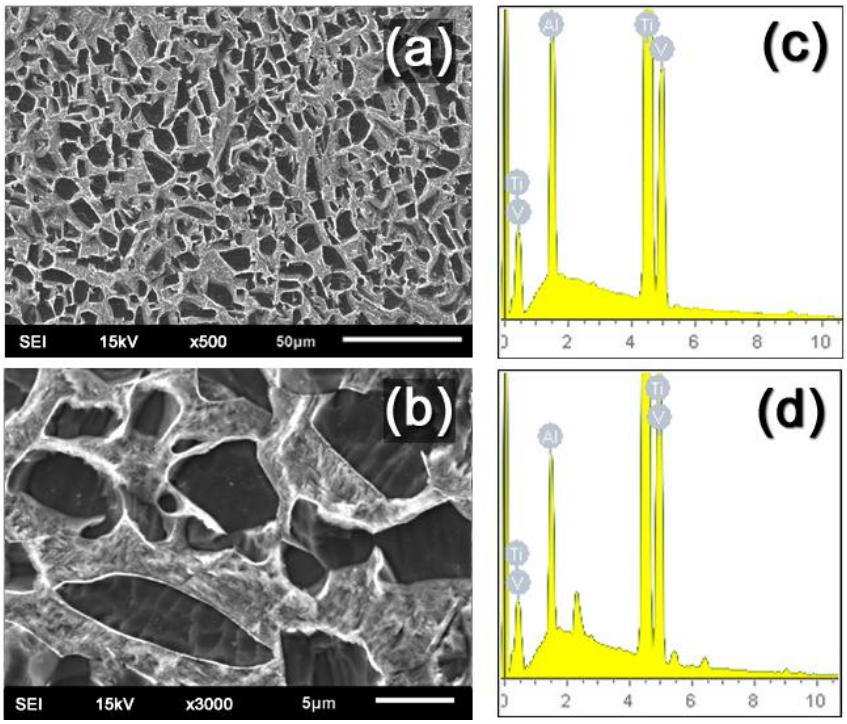

Figure 12. SEM/EDX for the as-annealed Ti-54M sample at 940 °C and after five days of immersion in 2 M HCl solutions, (**a**,**b**) are the SEM images; (**c**,**d**) are the EDX profiles for the area shown in (**a**,**b**), respectively.

The SEM images obtained for the Ti-54M alloy that was heat treated at 800 °C (Figure 11) showed that the surface has, unexpectedly, many pits, which were most probably due to a harsh localized attack towards that surface of the alloy via the chloride ions present in the acid molecules. The EDX spectra detected that the weight percentages of the elements found outside the pits (most of the surface) has 92.93% Ti, 4.55% Al, and 2.51% V, which represents the main elements of the Ti-54M alloy. On the other hand, the weight percentages for the elements found inside the pits (white areas) were 87.50% Ti, 3.69% Al, 5.97% V, 1.74% Mo, and 1.11% Fe. The elements found inside the pits indicate that the pits were filled with corrosion products, which were deposited after the dissolution of the main elements of the alloy.

The SEM micrographs obtained for Ti-54M alloy that was heat treated at 940 °C (Figure 12) showed clearly that the surface has two distinguished areas; dark and bright ones. The dark regions consist mainly of the original percentages of the elements of the alloy, where the weight percent of Ti was 92.87, Al was 5.75, and V was 1.37. The bright regions were similar to a net on the surface of the alloy and composed of 89.56% Ti, 3.07% Al, and 7.37% V in weight.

4. Conclusions

The corrosion behavior of hot swaged Ti-54M alloy in 2 M HCl solutions was reported. The effect of annealing temperature, namely, at 800 °C and 940 °C on the corrosion of the alloy in the acid solution, was also investigated. It has been found that the corrosion resistance of Ti-54M alloy is high against the harsh effect of the concentrated acid solutions. Annealing the alloy at 800 °C further increases the resistance against uniform corrosion, but allows the alloy to corrode via pitting attack. Increasing the annealing temperature to 940 °C remarkably increases the corrosion resistance of the Ti-54M alloy towards both uniform and pitting corrosion. Results together were in good agreement with each other and indicated that increasing the annealing temperature decreases the corrosion current and corrosion rate, and increases the polarization resistance. This effect was also found to decrease the absolute values of currents recorded for the alloy at a more active potential, 1.4 V (Ag/AgCl).

Acknowledgments: This project was supported by King Saud University, Deanship of Scientific Research, College of Engineering Research Center. The authors would also like to thank Twasol Research Excellence Program (TRE Program), King Saud University, Riyadh, Saudi Arabia for support.

Author Contributions: El-Sayed M. Sherif contributed reagents/materials/analysis tools, designed the experimental work and edited the final version of the paper; Ehab A. Danaf delivered the samples and helped in writing the draft version of the manuscript, Hany S. Abdo did the experimental work to corrosion and surface analysis; Sherif Zein El Abedin analyzed the data and wrote the draft version of the manuscript; Hasan Al-Khazraji delivered the samples and helped in writing the draft version of the manuscript.

Conflicts of Interest: The authors declare no conflict of interest.

References

1. Geetha, M.; Singh, A.K.; Asokamani, R.; Gogia, C. Ti based biomaterials, the ultimate choice for orthopaedic implants—A review. *Prog. Mater. Sci.* **2009**, *54*, 397–425. [CrossRef]
2. AlOtaibi, A.; El-Sayed, M.S.; Zinelis, S.; Al Jabbari, Y. Corrosion Behavior of Two cp Titanium Dental Implants Connected by Cobalt Chromium Metal Superstructure in Artificial Saliva and the Influence of Immersion Time. *Int. J. Electrochem. Sci.* **2016**, *11*, 5877–5890. [CrossRef]
3. Veiga, C.; Davim, J.P.; Loureiro, A.J.R. Properties and Applications of Titanium Alloys—A brief Review. *Adv. Mater. Sci.* **2012**, *32*, 133–148.
4. Boyer, R.-R. Titanium for Aerospace: Rationale and applications. *Adv. Perform. Mater.* **1995**, *2*, 349–368. [CrossRef]
5. Seikh, A.H.; Mohammad, A.; El-Sayed, M.S.; Al-Ahmari, A. Corrosion Behavior in 3.5% NaCl Solutions of γ-TiAl Processed by Electron Beam Melting Process. *Metals* **2015**, *5*, 2289–2302. [CrossRef]
6. Gopi, D.; El-Sayed, M.S.; Rajeswari, D.; Kavitha, L.; Pramod, R.; Dwivedi, J.; Polaki, S.R. Evaluation of the mechanical and corrosion protection performance of electrodeposited hydroxyapatite on the high energy electron beam treated titanium alloy. *J. Alloy. Compd.* **2014**, *616*, 498–504. [CrossRef]

7. The Mechanical and Ballistic Properties of an Electron Beam Single Melt of Ti-6A1-4V Plate. Available online: www.arl.army.mil/arlreports/2001/ARL-MR-515.pdf (accessed on 12 January 2017).
8. Machado, A.R.; Wallbank, J. Machining of titanium and its alloys—A review. *Proc. Inst. Mech. Eng. Part B J. Eng. Manuf.* **1990**, *204*, 53–60. [CrossRef]
9. Rahman Rashid, R.A.; Sun, S.; Wang, G.; Dargusch, M.S. Machinability of a near beta titanium alloy. *Proc. Inst. Mech. Eng. Part B J. Eng. Manuf.* **2011**, *225*, 2151–2162. [CrossRef]
10. Armendia, M.; Garay, A.; Iriarte, L.M.; Arrazola, P.-J. Comparison of the machinabilities of Ti6Al4V and TIMETAL® 54M using uncoated WC-Co tools. *J. Mater. Process. Technol.* **2010**, *210*, 197–203. [CrossRef]
11. Khanna, N.; Garay, A.; Iriarte, L.M.; Soler, D.; Sangwan, K.S.; Arrazola, P.J. Effect of heat treatment conditions on the machinability of Ti64 and Ti54M alloys. *Proced. CIRP* **2012**, *1*, 477–482. [CrossRef]
12. Khanna, N.; Sangwan, K.S. Cutting tool performance in machining of Ti555.3, Timetal®54M, Ti 6–2-4–6 and Ti 6–4 alloys: A review and analysis. In Proceedings of the 2nd CIRP International Conference on Process Machine Interactions, Vancouver, BC, Canada, 10–11 June 2010.
13. Khanna, N.; Sangwan, K.S. Comparative machinability study on Ti54M titanium alloy in different heat treatment conditions. *Proc. Inst. Mech. Eng. Part B J. Eng. Manuf.* **2013**, *227*, 96–101. [CrossRef]
14. Gabriela, S.B.; Dille, J.; Rezende, M.C.; Mei, P.; de Luiz, H.A.; Baldan, R.; Nunes, C.A. Mechanical Characterization of Ti–12Mo–13Nb Alloy for Biomedical Application Hot Swaged and Aged. *Mater. Res.* **2015**, *18*, 8–12. [CrossRef]
15. Al-Khazraji, H.; El-Danaf, E.; Wollmann, M.; Wagner, L. Microstructure, Mechanical, and Fatigue Strength of Ti-54M Processed by Rotary Swaging. *J. Mater. Eng. Perform.* **2015**, *24*, 2074–2084. [CrossRef]
16. Divi, S.; Grauman, J. Electrochemical Corrosion Properties of TIMETAL®54M. In Proceedings of the 13th World Conference on Titanium, San Diego, CA, USA, 16 August 2015.
17. ALkhazraji, H.; El-Danaf, E.; Wollmann, M.; Wagner, L. Enhanced Fatigue Strength of Commercially Pure Ti Processed by Rotary Swaging. *Adv. Mater. Sci. Eng.* **2015**, *2015*, 301837. [CrossRef]
18. Sherif, E.-S.M.; Potgieter, J.H.; Comins, J.D.; Cornish, L.; Olubambi, P.A.; Machio, C.N. Effects of minor additions of ruthenium on the passivation of duplex stainless steel corrosion in concentrated hydrochloric acid solutions. *J. Appl. Electrochem.* **2009**, *39*, 1385–1392. [CrossRef]
19. Latief, F.H.; El-Sayed, M.S. Effects of sintering temperature and graphite addition on the mechanical properties of aluminum. *J. Ind. Eng. Chem.* **2012**, *18*, 2129–2134. [CrossRef]
20. Sherif, E.-S.M. Electrochemical investigations on the corrosion inhibition of aluminum by 3-amino-1,2,4-triazole-5-thiol in naturally aerated stagnant seawater. *J. Ind. Eng. Chem.* **2013**, *19*, 1884–1889. [CrossRef]
21. Sherif, E.-S.M.; Ammar, H.R.; Khalil, K.A. A comparative study on the electrochemical corrosion behavior of microcrystalline and nanocrystalline aluminum in natural seawater. *Appl. Surf. Sci.* **2014**, *301*, 775–785.
22. Potgieter, J.H.; Olubambi, P.A.; Cornish, L.; Machio, C.N.; Sherif, K.A. Influence of nickel additions on the corrosion behaviour of low nitrogen 22% Cr series duplex stainless steels. *Corros. Sci.* **2008**, *50*, 2572–2579. [CrossRef]
23. Roberge, P.R. *Handbook of Corrosion Engineering*; McGrow-Hill: New York, NY, USA, 2000.
24. Sherif, E.M.; Park, S.-M. Inhibition of copper corrosion in acidic pickling solutions by *N*-phenyl-1,4-phenylenediamine. *Electrochim. Acta* **2006**, *51*, 4665–4673. [CrossRef]
25. Scully, J.R. Polarization resistance method for determination of instantaneous corrosion rates. *Corrosion* **2000**, *56*, 199–218. [CrossRef]